

New Europium(III)-TTA Complex Containing 2-Pyrrolidone as Coligand to Application as Luminescent Sensor: Pb^{II} and Ethanol in Gasoline

Clebson J. Macrino,^{1b a,b} Alex S. Borges,^c Álvaro Cunha Neto,^{1b a}
Valdemar Lacerda Jr.^{1b *,a} and Wanderson Romão^{1b *,a,b,d}

^aLaboratório de Petroleômica e Forense, Universidade Federal do Espírito Santo (UFES),
Avenida Fernando Ferrari, 514, Goiabeiras, 29075-910 Vitória-ES, Brazil

^bInstituto Nacional de Ciência e Tecnologia Forense (INCT Forense),
Av. Ipiranga, 6681, Partenon, 90619-900 Porto Alegre-RS, Brazil

^cInstituto Federal do Espírito Santo (IFES), Av. Vitória, Jucutuquara, 29040-780 Vitória-ES, Brazil

^dInstituto Federal do Espírito Santo (IFES), Av. Ministro Salgado Filho, Soteco,
29106-010 Vila Velha-ES, Brazil

This work describes the synthesis and application of an europium(III) complex, [Eu(TTA)₃(2-pyr)(H₂O)], containing 2-thenoyltrifluoroacetate (TTA) and 2-pyrrolidone (2-pyr) as ligands, obtained as white solid and soluble in ethanol. In solution, the complex showed red emission, characteristic of the Eu^{III} emission in the solid state ($\lambda_{exc} = 375$ nm and $\lambda_{em} = 612$ nm). The complex was tested with Pb^{II}, Cd^{II}, and Hg^{II} ions in water. The effect of metal ions was monitored and evaluated by hypersensitive transition $^5D_0 \rightarrow ^7F_2$ (612 nm). The results show that Pb^{II} suppresses the complex luminescence and present high sensitivity, according to the values for the Stern-Volmer constant ($K_{SV} = 2300$ L mol⁻¹), showing good linearity, i.e., determination coefficient (R^2) of 0.9913, and low limit of detection (LOD = 6.03 μ M). Luminescence quenching increased with the increasing concentration of Pb^{II}. These results indicate that the synthesized complex is a potential luminescent sensor for detecting Pb^{II} in a simple and fast way, being applicable for routine environmental analysis. When applied as an ethanol sensor in gasoline, the complex hypersensitive transition intensity decreased with the increasing volume of ethanol in gasoline, reaching the values of $R^2 = 0.9815$ and LOD = 4.94% v/v.

Keywords: europium(III), 2-pyrrolidone, lanthanides, luminescent sensor

Introduction

Due to their luminescent properties, lanthanide ions compounds arouse the interest of the industry in developing new technologies.¹⁻⁸ Lanthanides are particularly interesting for the spectroscopic properties of their trivalent ions, resulting from the 4f-4f electron transition.⁹ Although prohibited by the Laporte rule, the Judd-Ofelt theory postulates that these transitions occur due to the influence of coordination geometrical symmetry, which in most cases has asymmetric structures.¹⁰ The coordination number of lanthanide compounds is usually greater than six,¹¹⁻¹³ presenting point groups with coordination number equal to seven, such as mono-capped octahedron (C_{3v}) or a mono-

capped trigonal prism (C_{2v}),¹⁴ equal to eight, such as square antiprism (D_{4d}) and bi-capped trigonal prism (C_{2v}),¹⁵ or even equal to nine, as occurs with tri-capped trigonal prism (C_{3h}) or capped square antiprism (C_{4v}).^{16,17}

As f orbitals are shielded by the 5s and 5p orbitals, 4f-4f transitions are little influenced by the ligand field, generating narrow-band emissions similar to those of the free metal, which are always located in the same region.¹⁸

Lanthanides have a low molar absorption coefficient. As the direct excitation of lanthanide ion is not very efficient for emitting light, the use of ligands is necessary to perform the ligand to metal energy transfer process known as the antenna effect.¹⁹⁻²¹

From this process, the energy absorbed by the ligand passes from low-energy singlet to the high-energy singlet (S₀ → S₁), possibly involving an intersystem crossing of the high energy singlet to the triple excited state of the ligand

*e-mail: vljuniorqui@gmail.com; wandersonromao@gmail.com

Editors handled this article: Jáfisa Fernandes Soares and Humberto O. Stumpf (Associate)

($S_0 \rightarrow T_1$). Thus, this process may imply energy transfer from S_1 or T_1 to each emitting level of the lanthanide, especially regarding the triplet state for having a relative longer lifetime.²²⁻²⁵ Among the lanthanides, Eu^{III} ions are capable of emitting red light, Tb^{III} green light, Sm^{III} orange light, and Tm^{III} blue light in the visible region, whereas Dy^{III} and the Sm^{III} emit lights in the near-infrared region.²⁶⁻³²

In its excited state ($^5\text{D}_0$ ca. 17267 cm^{-1}), the Eu^{III} ion have lower energies than most organic ligand triplet states, thus being widely used.³³ Likewise, β -diketones ligands are among the most used to obtain compounds with high light emission efficiency since their structures present chelating capacities and are favored by the $\pi \rightarrow \pi^*$ transitions.³⁴⁻⁴⁰

The literature reported many luminescent lanthanide compounds for various applications. Lucena *et al.*⁴¹ reported a $\text{ZnAl}_{1.95}\text{Ln}_{0.05}\text{O}_4$ (where $\text{Ln} = \text{Eu}^{\text{III}}$ or Tb^{III}) enabled the marking of ammunition and clearly identified luminescent gunshot residue (GSR). The identification can be performed visually by direct UV irradiation of any surface containing GSR particles. Destefani *et al.*⁴² reported the evaluation of acute toxicity of the complex $[\text{Eu}(\text{PIC})_3(\text{NMK})_3]$, which has as ligands picric acid (PIC) and *N*-methyl-caprolactam (NMK), applied as luminescent marker for the visual identification of GSR. Devi *et al.*⁴³ synthesized a series of smart luminescent Eu^{III} complexes with five different ligands $[\text{Eu}(\text{DBM})_3(\text{ligand})]$ using functionalized phenanthro-imidazole derivatives as the neutral ligands and dibenzoylmethanate (DBM) as the anionic ligand and red light-emitting diodes (LEDs) were fabricated by integrating a near-ultraviolet (NUV). Wang *et al.*⁴⁴ reported europium(III) chelated nanoparticles (EuNPs) conjugated to monoclonal antibodies specific to the O-specific polysaccharide fractions of *Escherichia coli* O157:H7. The EuNPs were used as fluorescent nanoparticle immunochromatographic strips, which enable rapid and quantitative detection in food samples. Zmojda *et al.*⁴⁵ reported luminescent studies on germanate glasses doped with Eu^{III} ions for photonic applications. Zhang *et al.*⁴⁶ reported a biodegradable film enabling visible light excitation of hexanuclear Eu^{III} complex $[\text{Eu}_6(\text{TTA})_{18}\text{CTP-TPY}]$ (TTA = 2-thenoyltrifluoroacetone; CTP-TPY = 2,2,4,4,6,6-hexakis(4-((2,2':6',2''-terpyridin)-4'-yl)phenoxy)-1,3,5,2- λ^5 ,4 λ^5 ,6 λ^5 -triazatriphosphinine) for various applications. Li *et al.*⁴⁷ synthesized a luminescent europium metal-organic framework $[\text{Eu}(\text{Hbptc})(\text{H}_2\text{O})_3]_n$ (Hbptc = biphenyl-2,3,3',5'-tetracarboxylate) for selective sensing of pollutant small organic molecules. Zhou *et al.*⁴⁸ reported a ZnSe quantum dot based ion imprinting technology for fluorescence detecting Cd^{II} and Pb^{II} ions on a 3D rotary paper based microfluidic chip. Sun *et al.*⁴⁹ reported a lanthanide metal-organic frameworks (Ln-MOFs)

$\{[\text{Ln}(\text{L})(\text{ox})_{0.5}(\text{H}_2\text{O})_2] \cdot \text{H}_2\text{O}\}_n$ ($\text{Ln} = \text{Pr}, \text{Nd}, \text{Sm}$ and Eu) constructed by 5-hydroxyisophthalic acid (H_2L) and oxalate (ox) through solvothermal methods as luminescent sensor to acetone and Cu^{II} . Chen *et al.*⁵⁰ synthesized a three lanthanide metal-organic frameworks (LnMOFs) $[\text{Ln}_2\text{L}_3(\text{H}_2\text{O})_2]_n$ ($\text{Ln}^{\text{III}} = \text{Eu}^{\text{III}}, \text{Tb}^{\text{III}}$ and Gd^{III}) adopting the ligand of cyclobutane-1,1-dicarboxylic acid (H_2L). The study indicates that Eu^{III} complex is a luminescence sensor for methanol. Zhang *et al.*⁵¹ reported a lanthanide MOF (LnMOF) of $[\text{Tb}(\text{HIP})(\text{H}_2\text{O})_5] \cdot (\text{H}_2\text{O}) \cdot (\text{HIP})_{1/2}$ (Tb-HIP, where HIP is 5-hydroxyisophthalate) for detecting picric acid and macrodantin. Zhai *et al.*⁵² reported an europium metal-organic framework (Eu-MOF), $[\text{Eu}(\text{L})(\text{OAc})(\text{DMA})]_n$ (DMA = *N,N*-dimethylacetamide) as luminescent probe for detecting Al^{III} . Li *et al.*⁵³ reported lanthanide polymers $\{[\text{Ln}_2(\text{bpda})_3(\text{H}_2\text{O})_3] \cdot \text{H}_2\text{O}\}_n$ ($\text{Ln} = \text{Tb}$ or Dy) that have been synthesized with 2,2'-bipyridine-4,4'-dicarboxylic acid (H_2bpda) as fluorescent sensor to Hg^{II} . Zheng *et al.*⁵⁴ synthesized an europium based metal-organic framework (Eu-MOF), EuL_3 ($\text{L} = 4'-(4\text{-carboxyphenyl})-2,2':6',2''\text{-terpyridine}$), under hydrothermal conditions, and used it as a solid luminescence sensor for Fe^{III} . Yan *et al.*⁵⁵ synthesized an oleic acid (OA)-capped $\beta\text{-NaYF}_4: 20\% \text{Yb}, 0.5\% \text{Tm}$ upconversion nanoparticles (UCNPs) [OA-UCNPs] for Cu^{II} sensing. Xu *et al.*⁵⁶ reported a Eu^{III} functionalized Zr-based metal-organic framework as fluorescent probe for Cd^{II} detection in aqueous environment. Lou *et al.*⁵⁷ reported a "blue-to-red" colorimetric method for determination of Hg^{II} and Ag^{I} based on stabilization of gold nanoparticles (AuNPs) by redox formed metal coating in the presence of ascorbic acid (AA). Lian *et al.*⁵⁸ reported a $\{[\text{Yb}(\text{TTTTPC}) \cdot (\text{H}_2\text{O})_2] \cdot 3\text{Cl} \cdot \text{NO}_3 \cdot 0.5\text{DMA} \cdot 6\text{H}_2\text{O}\}_n$ synthesized in conventional aqueous solutions with H_3TTTTPC ligands ($\text{H}_3\text{TTTTPC} = 1,1',1''-(2,4,6\text{-trimethylbenzene-1,3,5-triyl(methylene))-tris(pyridine-4-carboxylic acid)}$), DMA = *N,N*-dimethylacetamide) for highly selective and sensitive luminescent sensor for Pb^{II} over mixed metal ions. Yang *et al.*⁵⁹ synthesized nanoporous coordination polymers $\{[\text{La}_2(\text{PDA})_3(\text{H}_2\text{O})_4] \cdot \text{H}_2\text{O}\}_\infty$ (PDA = pyridine-2,6-dicarboxylate) and $\{[\text{Pr}_2(\text{PDA})_3(\text{H}_2\text{O})_3] \cdot \text{H}_2\text{O}\}_\infty$ as selective luminescent probes of Pb^{II} , Ca^{II} and Cd^{II} ions. Fonseca *et al.*⁶⁰ reported a terbium(III)-based metal-organic framework as a luminescent sensor to detect the adulteration of ethanol fuel with methanol.

The literature reported the great versatility of the use of lanthanides with 2-thenoyltrifluoroacetone (TTA) and others coligands. Xue *et al.*⁶¹ reported lanthanide complexes $[\text{Yb}(\text{fac})_3(\text{H}_2\text{O})_2]$, $[\text{Yb}(\text{TTA})_3(\text{H}_2\text{O})_2]$, $[\text{Nd}(\text{TTA})_3(\text{H}_2\text{O})_2]$ (fac = 1,1,1,5,5,5-hexafluoro-2,4-pentanedione) functionalized nanofibrillated cellulose (Ln-NFC) nanopapers with near-infrared (NIR) luminescence to bring

a brilliant future for UV filters. Teotonio *et al.*⁶² reported a [Eu(TTA)₂(NO₃)(TPPO)₂] (TPPO = triphenylphosphine oxide) (bis-TTA complex) and [Eu(TTA)₃(TPPO)₂] (tris-TTA complex) where was evaluated the photoluminescent and triboluminescent behavior. Li *et al.*⁶³ reported a novel organic-inorganic mesoporous luminescent hybrid containing Ln^{III} (Eu^{III}, Tb^{III}) complexes covalently attached to the functionalized ordered mesoporous SBA-15 (Santa Barbara amorphous-15), which were designated as Ln(TTA-SBA-15)₃bpy and Ln(DBM-SBA-15)₃bpy (bpy = 2,2'-bipyridine), respectively, obtained by sol-gel process. Li *et al.*⁶⁴ synthesized nanocomplexes NaGdF₄:Yb,Er@SiO₂@Eu(TTA)₃Phen (2-thenoyltrifluoroacetone, TTA), (1,10-phenanthroline monohydrate, Phen) showing the ligand-sensitized Eu^{III} complexes attached to the outer surface of SiO₂. The green (542 nm) and red (610 nm) light were excited by NIR and UV illumination, respectively. In this context, this work uses a Eu^{III} compound with 2-thenoyltrifluoroacetate (TTA) and 2-pyrrolidone (2-pyr) ligands as a luminescent sensor to identify Pb^{II} in water and ethanol in gasoline.

Experimental

Materials

Europium(III) oxide (Eu₂O₃) and the ligands 2-thenoyltrifluoroacetate (TTA = C₈H₄F₃O₂S) and 2-pyrrolidone (2-pyr = C₄H₇NO) were purchased from Sigma-Aldrich (St. Louis, MO, USA). Eu₂O₃ was converted to its respective chloride using concentrated hydrochloric acid.³⁹

Characterization of complex

The europium(III) compound with TTA, [Eu(TTA)₃(H₂O)₂], was synthesized according to an adapted literature procedure.⁶⁵ The percentage of europium in the complex was determined by complexometric titration with 0.01 mol L⁻¹ standard EDTA (ethylenediamine tetraacetic acid) solution using *ortho*-xylenol orange as indicator. Carbon, hydrogen, and nitrogen (CHN) elemental analysis was performed using the PerkinElmer 2400 series II Elemental Analysis Instrument (Waltham, Massachusetts, USA). Infrared spectra were obtained from the spectral region of 4000 to 400 cm⁻¹ using a KBr tablet in transmittance mode and a PerkinElmer FTIR GX spectrometer (Waltham, Massachusetts, USA) at room temperature. Thermogravimetry analysis (TGA) was performed using a TG 60-H Shimadzu thermobalance (Kyoto, Japan) at a flow rate of 50 mL min⁻¹ and a heating rate of 10 °C min⁻¹, under the temperature range of 25 to

800 °C and ambient atmosphere. Solid-state Ultraviolet-Visible (UV-Vis) spectroscopy analysis was performed in the 200-800 nm region using a PerkinElmer spectrometer (Waltham, Massachusetts, USA). Photoluminescence spectra (excitation and emission) were obtained using a FLUOROLOG3 ISA/JobinYvon Horiba (Edison, New Jersey, USA) spectrofluorometer equipped with a Hamamatsu R928P photomultiplier, the SPEX 1934 D phosphorimeter, a 450 W Xe lamp, and a pulsed 150 W Xe-Hg lamp.

Synthesis of the [Eu(TTA)₃(2-pyr)(H₂O)] complex

[Eu(TTA)₃(2-pyr)(H₂O)] was synthesized according to an adapted literature procedure.⁴⁰ First, 2-pyr (0.20 g, 2.35 mmol) was added dropwise to a methanol solution (30 mL) of [Eu(TTA)₃(H₂O)₂] (1.20 g, 1.40 mmol) and left stirring overnight. The resulting white solid was washed with water to remove the excess 2-pyr ligand, dried, and stored at room temperature. The scheme represents the synthesis of the complex (Figure 1).

Selectivity study of metals

Ions from heavy metals are major pollutants, posing significant risks both to human health and the environment. Ions such as Ni^{II}, Hg^{II}, Zn^{II}, Cd^{II}, Pb^{II}, Cu^{II}, and Cr^{IV} are not easily degraded when compared to conventional organic pollutants. Most of them are highly toxic and cancerous, raising concern due to their cumulative capacity in living organisms.^{66,67} Considering that, we investigated the effect of metal ions on the luminescence of the [Eu(TTA)₃(2-pyr)(H₂O)] complex using three heavy metals, namely Pb^{II}, Cd^{II}, and Hg^{II}. For each metal, aqueous solutions were prepared from their respective nitrates in a 2.41 × 10⁻³ mol L⁻¹ concentration. An ethanolic solution of the complex was also prepared in a 6.50 × 10⁻⁵ mol L⁻¹ concentration. Then, 0.500 mL of each metal aqueous solution was individually mixed with 2.500 mL of the solution containing [Eu(TTA)₃(2-pyr)(H₂O)]. The mixtures were stirred and analyzed in the spectrofluorometer.

Detection of ethanol content in gasoline

Type 'A' gasoline (without additives) and ethanolic solution of the complex in the concentration of 6.50 × 10⁻⁵ mol L⁻¹ were used in the experiment. Gasoline was mixed with ethanol in proportions ranging from 0-100% (v/v), stirred, and analyzed on the spectrofluorometer. This experiment sought to evaluate the behavior of the ethanol/complex when mixed with gasoline to verify whether

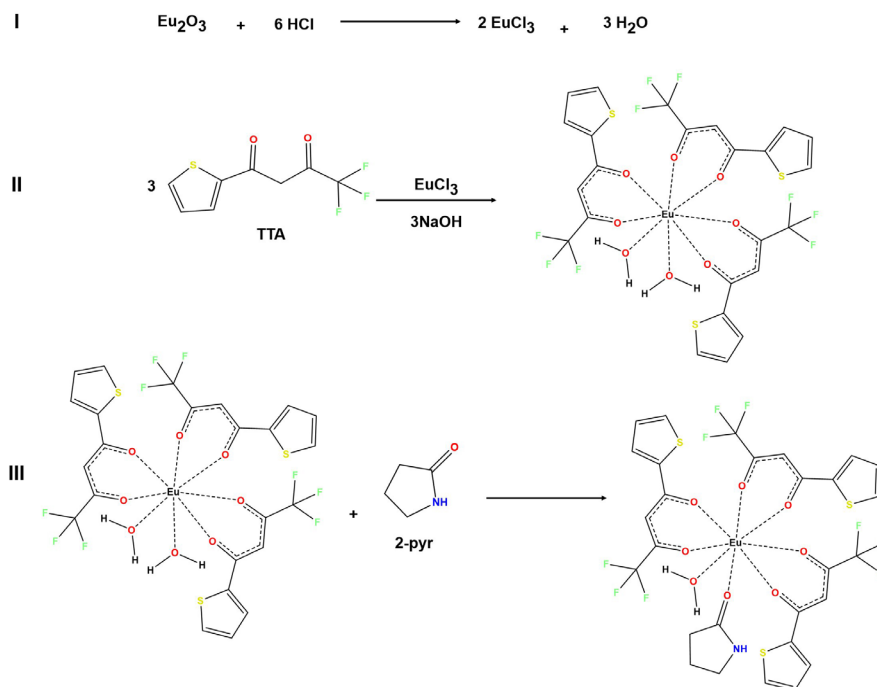


Figure 1. Synthetic route of $[\text{Eu}(\text{TTA})_3(2\text{-pyr})(\text{H}_2\text{O})]$.

it would be applicable as a luminescent sensor for identifying gasoline adulteration by photoluminescence.

Results and Discussion

Characterization of $[\text{Eu}(\text{TTA})_3(2\text{-pyr})(\text{H}_2\text{O})]$

The results obtained from carbon, hydrogen, and nitrogen (CHN) elemental analysis and complexometric EDTA titration⁶⁸ suggest the formation of the stoichiometric compound $[\text{Eu}(\text{TTA})_3(2\text{-pyr})(\text{H}_2\text{O})]$.

$\text{C}_{28}\text{H}_{21}\text{EuF}_9\text{NO}_8\text{S}_3$ calcd. (%): Eu^{III} 16.49, C 35.98, H 2.24, N 1.45, measured: Eu^{III} 16.54, C 36.61, H 2.30, N 1.52; FTIR ν/cm^{-1} (Figure S1, Supplementary Information (SI) section) $\nu_{\text{ass}}\text{C}-\text{O}$ (1536_{(s)}}), $\nu_{\text{s}}\text{C}-\text{O}$ (1623_{(s)}}), $\nu\text{C}-\text{N}$ (1496_{(s)}}); TTA free: $\nu_{\text{s}}\text{C}-\text{O}$ (1654_{(s)}}) and 2-pyr free: $\nu_{\text{s}}\text{C}-\text{O}$ (1662_{(s)}}), $\nu\text{C}-\text{N}$ (1467_{(s)}}). Molar conductance in acetonitrile: 4.41 $\text{cm}^2 \Omega^{-1} \text{mol}^{-1}$. Yield 85%. Based on the molar conductance in acetonitrile, we may rightfully infer that the compound is nonelectrolyte, thus indicating that the three TTA are linked to the first coordination sphere of the complex, similarly to the $[\text{Eu}(\text{TTA})_3(\text{NMC})(\text{H}_2\text{O})]$ (NMC = *N*-methyl- ϵ -caprolactam) studied by Borges *et al.*^{39,40}

The Fourier transformed infrared spectroscopy (FTIR) (Figure S1) showed that the band associated with the symmetrical stretch, $\nu_{\text{s}}\text{C}-\text{O}$ in 1623 cm^{-1} , suffered a shift to lower wavenumbers concerning the TTA (1654 cm^{-1}) and 2-pyr (1643 cm^{-1}), suggesting a coordination with Eu^{III} ion. The $[\text{Eu}(\text{TTA})_3(2\text{-pyr})(\text{H}_2\text{O})]$ complex also presented

the band associated with the asymmetric stretch, $\nu_{\text{ass}}\text{C}-\text{O}$ (1536 cm^{-1}), absent in the free ligand spectra, corroborating with ligands coordination. Both TTA and 2-pyr present $\nu\text{C}=\text{O}$, but they cannot be distinguished because they occur in the same region. The presence of the stretch vibration $\nu\text{C}-\text{N}$ and its wavenumbers shift to larger values concerning free 2-pyrrolidone ligand suggests that this ligand is coordinated. Thus, the $\nu_{\text{s}}\text{C}-\text{O}$ displacement in TTA and 2-pyr suggest that these ligands are coordinated by carbonyl oxygen. Also, the spectrum of the complex presented the characteristic water $\nu\text{O}-\text{H}$ vibrational mode in the 3000-3500 cm^{-1} region, suggesting the presence of water.⁶⁹

The thermogravimetry analysis (Figure S2, SI section) presented three main events of mass loss. From 25 to 76 °C, the compound is very stable. The first mass loss occurred from 76 to 120 °C, as an endothermic event. This first stage was related to the water output of coordination (experimental: 1.98%, calculated: 1.96%), corroborating the suggested stoichiometry. The following two steps are exothermic and occurred with peak temperatures at 289 and 456 °C, related to the thermal degradation of organic ligands, 2-tenoiltrifluoroacetone and 2-pyrrolidone. The second weight loss (58.99%) occurred from 120 to 395 °C, which was attributed to the decomposition of two TTA and 2-pyr molecules. The third stage with about 20.91% mass loss started at 395 °C, finished at 540 °C, the mass loss percentage was near the loss of one TTA molecule from the complex. Complete degradation of the Eu^{III} complex

occurs at 540 °C, with a total mass loss of 81.88% (residue mass: 18.12%). The total mass loss calculated was 80.99%, considering that the residue is Eu_2O_3 (calculated: 19.01%).

The absorption spectrum in the ultraviolet-visible (UV-Vis) region (Figure S3, SI section) showed bands with maximum absorption at 268 nm, attributable to $\pi \rightarrow \pi^*$ intraligand electronic transitions, and an intense band in the 330 nm region, attributable to $n \rightarrow \pi^*$ transitions. The excitation spectrum (Figure 2a) showed an intense broad band in the 250-450 nm assigned to $S_0 \rightarrow S_1$ and bands assigned to the 4f-4f transitions overlapped by the ligand band. The 4f-4f transitions are originated from the 7F_0 ground state to the excited levels 5L_J : 5L_9 (360 nm), 5H_4 (379 nm), 5L_7 (385 nm), 5L_6 (393 nm) and 5D_3 (415 nm) excited states and remain approximately invariable in each Eu^{III} complex. So, the 4f-4f transitions overlapped by the ligand band can be also an efficient channel for the photoluminescence for the compounds.⁷⁰ And it is possible to identify the bands ${}^7F_0 \rightarrow {}^5D_3$ (451 nm), ${}^7F_0 \rightarrow {}^5D_2$ (466 nm), ${}^7F_0 \rightarrow {}^5D_1$ (526 nm), ${}^7F_0 \rightarrow {}^5D_0$ (580 nm).⁴⁰

At room temperature, the emission spectrum (Figure 2b) of the compound in solid-state showed the regions of the intraconfigurational transitions, ${}^5D_0 \rightarrow {}^7F_J$ ($J = 0, 1, 2, 3$, and 4), with maximum emission at 612 nm, ${}^5D_0 \rightarrow {}^7F_2$ followed by 591 nm, ${}^5D_0 \rightarrow {}^7F_1$, 652 nm, ${}^5D_0 \rightarrow {}^7F_3$, and 700 nm, ${}^5D_0 \rightarrow {}^7F_4$. The presence of the ${}^5D_0 \rightarrow {}^7F_2$ transition, a hypersensitive electric dipole transition whose intensity is higher than that of ${}^5D_0 \rightarrow {}^7F_1$ (allowed by a magnetic dipole transition), suggests that the compound does not have an inversion center and that Eu^{III} is in chemical environment of low symmetry.⁷¹ Experimental intensity parameters, Ω_λ , for the $[\text{Eu}(\text{TTA})_3(2\text{-pyr})(\text{H}_2\text{O})]$ complex were determined from the emission spectra using the following equation 1.⁷²

$$\Omega_\lambda = \frac{4e^2\omega^3 A_{0\lambda}}{3\hbar c^3 \chi^7 F_J \parallel U^{(\lambda)} \parallel {}^5D_0^2} \quad (1)$$

where e is the electron elementary charge, ω is the angular frequency, \hbar is the Planck's constant divided by 2π , c is the

speed of light and χ is the Lorentz local field correction term, given by $\chi = n(n^2 + 2)^2/9$ and ${}^7F_J \parallel U^{(\lambda)} \parallel {}^5D_0^2$ is a squared reduced matrix element with value of 0.0032 for the ${}^5D_0 \rightarrow {}^7F_2$ transition and 0.0023 for the ${}^5D_0 \rightarrow {}^7F_4$. The refractive index (n) has been assumed equal to 1.5. In this work, the ${}^5D_0 \rightarrow {}^7F_6$ transition was not observed experimentally, consequently, the experimental Ω_6 parameter could not be estimated. The spontaneous emission coefficient, $A_{01} = 0.31 \times 10^{-11}(n)^3(v_{01})^3$, leading to an estimated value around 50 s^{-1} for the refractive index (n) defined above.⁷² In equation 2, the A_{0j} term, where $J = 2$ and 4, represents the spontaneous emission coefficients of the ${}^5D_0 \rightarrow {}^7F_2$ and ${}^5D_0 \rightarrow {}^7F_4$ transitions, which can be calculated from ${}^5D_0 \rightarrow {}^7F_1$ reference transition (magnetic dipole mechanism), therefore this transition is practically insensitive to chemical environment changing, equation 2.⁷³

$$A_{0j} = \frac{\sigma_{0\lambda} S_{0\lambda}}{S_{01} \sigma_{0\lambda}} A_{01} \quad (2)$$

where S_{01} and $S_{0\lambda}$ are the areas under the curves of the ${}^5D_0 \rightarrow {}^7F_1$ and ${}^5D_0 \rightarrow {}^7F_j$ transitions, with σ_{01} and $\sigma_{0\lambda}$ being their energy barycenters, respectively.⁷³

The lifetimes (τ) of the $[\text{Eu}(\text{TTA})_3(2\text{-pyr})(\text{H}_2\text{O})]$ complex were obtained from the photoluminescence decay curves (Figure S4, SI section) using the equation $I(t) = I(0) \exp(-t/\tau)$ and a curve fitting program, where $I(t)$ is the intensity at time t , t is time and $I(0)$ is the intensity in the initial time equal to zero ($t = 0$). The quantum efficiency of the 5D_0 emitting level (η) for the Eu^{III} complex are presented in Table 1 and were calculated from the ratio $A_{\text{rad}}/A_{\text{total}}$, where A_{rad} and A_{total} are radiative and total rates assigned to the decay processes of the 5D_0 emitting level, respectively. In this case, the A_{rad} values were obtained by summing the radiative spontaneous coefficients due to the ${}^5D_0 \rightarrow {}^7F_j$ transitions, while A_{total} were determined from the lifetime values of the 5D_0 emitting level (τ) by considering the reciprocal relation between these properties ($A_{\text{total}} = 1/\tau$).⁷⁴

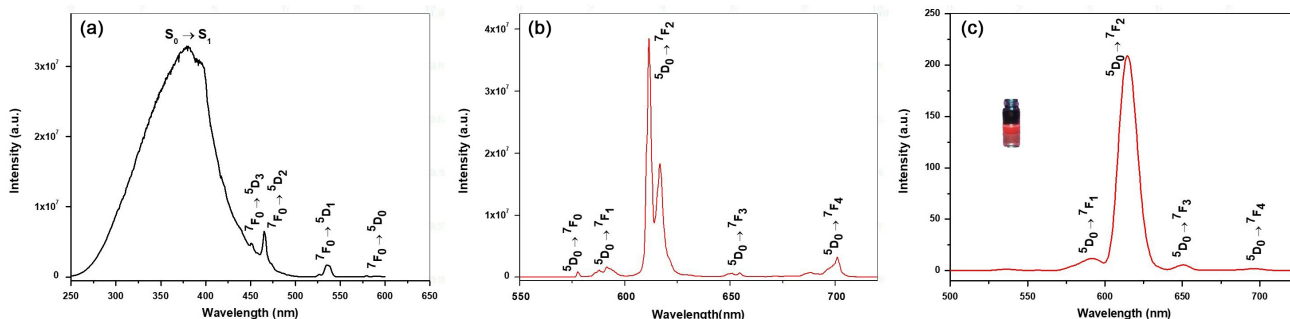


Figure 2. (a) Excitation, with $\lambda_{\text{exc}} = 612 \text{ nm}$, and (b) emission, with $\lambda_{\text{exc}} = 375 \text{ nm}$, spectra of the complex in solid-state, and (c) emission, with $\lambda_{\text{exc}} = 375 \text{ nm}$, spectra of the complex ($6.50 \times 10^{-5} \text{ mol L}^{-1}$) in ethanolic solution.

Table 1. Experimental values of intensity parameters (Ω_2), radiative (A_{rad}), nonradiative (A_{nrad}) rates, lifetimes (τ), emission quantum efficiencies (η) of the 5D_0 emitting level determined for complexes $[\text{Eu}(\text{TTA})_3(2\text{-pyr})(\text{H}_2\text{O})]$ and compared to literature

Complex	Ω_2 / cm^2	Ω_4 / cm^2	$A_{\text{rad}} / \text{s}^{-1}$	$A_{\text{nrad}} / \text{s}^{-1}$	τ / ms	$\eta / \%$	Reference
$[\text{Eu}(\text{TTA})_3(2\text{-pyr})(\text{H}_2\text{O})]$	23×10^{-20}	7×10^{-20}	886	1114	0.500	44	this work
$[\text{Eu}(\text{TTA})_3(\text{NMC})(\text{H}_2\text{O})]$	32×10^{-20}	7×10^{-20}	1147	2078	0.310	36	40
$[\text{Eu}(\text{TTA})_3(\text{H}_2\text{O})_2]$	33×10^{-20}	5×10^{-20}	1110	2796	0.256	28	40

TTA: 2-thenoyltrifluoroacetate; 2-pyr: 2-pyrrolidone; NMC: *N*-methyl- ϵ -caprolactam.

The Table 1 shows the experimental values, obtained from the emission spectra, for the quantum efficiency (η), radiative (A_{rad}) and nonradiative (A_{nrad}) rates of spontaneous emission, lifetimes (τ) and the Judd-Ofelt intensity parameters (Ω_2 and Ω_4), for the Eu^{III} ion in the complex.

The experimental data reveal that the substitution of the water molecule by a lactam increases the quantum efficiency of the europium complexes as noted by Borges *et al.*⁴⁰ The value of η determined for this complex ($\eta = 44\%$) is not larger owing to the presence of one water molecule in the first coordinated sphere of the Eu^{III} ion. This luminescence quenching is an effect of the vibronic coupling of the higher-energy OH oscillators and 5D_0 emitting level causing a non-radiative dissipation of the energy. When compared with another complex reported in the literature $[\text{Eu}(\text{TTA})_3(\text{NMC})(\text{H}_2\text{O})]$, changes occur in the radiative coefficient (A_{rad}), the values of η are mainly associated to changes in the non-radiative rates (A_{nrad}). The experimental intensity parameters Ω_2 and Ω_4 of $[\text{Eu}(\text{TTA})_3(2\text{-pyr})(\text{H}_2\text{O})]$ present different values from those of $[\text{Eu}(\text{TTA})_3(\text{NMC})(\text{H}_2\text{O})]$ synthesized by Borges *et al.*,⁴⁰ indicating that Eu^{III} ions are in different chemical environments (Table 1). According to the literature, the Ω_2 value is the most influenced by small angular changes in the local geometry. This effect, together with changes in the ligating atom polarizability (α), has been used to rationalize the hypersensitivity of certain 4f-4f transitions to changes in the chemical environment.⁴⁰

Selectivity study of metals

The emission spectrum of the mixture containing 2.50 mL of the complex in ethanolic solution and 0.500 mL of pure water (Figure 2c) showed the intraconfigurational transitions $^5D_0 \rightarrow ^7F_1$, $^5D_0 \rightarrow ^7F_2$, $^5D_0 \rightarrow ^7F_3$, and $^5D_0 \rightarrow ^7F_4$. We used the hypersensitive transition $^5D_0 \rightarrow ^7F_2$ (612 nm) as a reference to monitor possible metal-induced disturbances in the luminescence of the complex. As for the emission spectrum of the complex (Figure 3a), we verified that Pb^{II} decreased intensity by 12% at the reference transition (Figure 3b). Thus, the metal-induced luminescence quenching followed the order: $\text{Pb}^{\text{II}} > \text{Cd}^{\text{II}} > \text{Hg}^{\text{II}}$. The effect of Pb^{II} in the presence of other metals was evaluated by

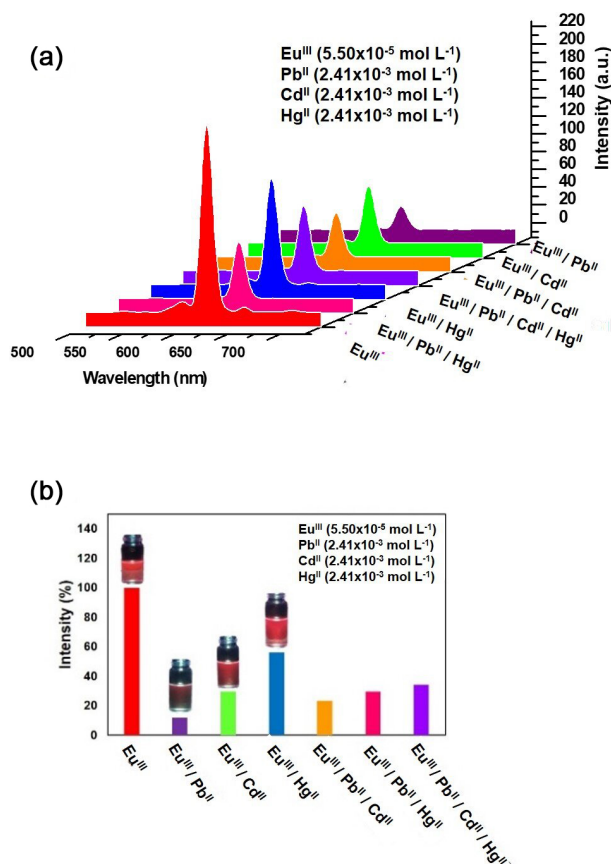


Figure 3. (a) Emission spectra ($\lambda_{\text{ex}} = 375$ nm) and (b) fluorescence intensity of the transition $^5D_0 \rightarrow ^7F_2$ (612 nm) of $[\text{Eu}(\text{TTA})_3(2\text{-pyr})(\text{H}_2\text{O})]$ in ethanol solution with Pb^{II} , Cd^{II} and Hg^{II} in aqueous solutions.

mixtures of 0.500 mL of each metal at the concentration of 2.41×10^{-3} mol L⁻¹, it was kept the same final volumes and equimolar concentrations of the ions to avoid the effect of dilution on luminescence.

Figure 3a shows that the luminescence intensity of the $[\text{Eu}(\text{TTA})_3(2\text{-pyr})(\text{H}_2\text{O})]$ solution decreases with all elements studied (Pb^{II} , Hg^{II} , and Cd^{II}). In the presence of Pb^{II} , the intensity of transition of Hg^{II} and Cd^{II} significantly decreases when compared to the elements alone.

We evaluated the change in luminescence intensity at 612 nm in the presence of Pb^{II} at different concentrations (1.45×10^{-4} , 2.42×10^{-4} , 4.83×10^{-4} , 7.25×10^{-4} , 9.66×10^{-4} , 1.93×10^{-3} and 2.41×10^{-3} mol L⁻¹) (Figure 4a) and found luminescence quenching to significantly increase with

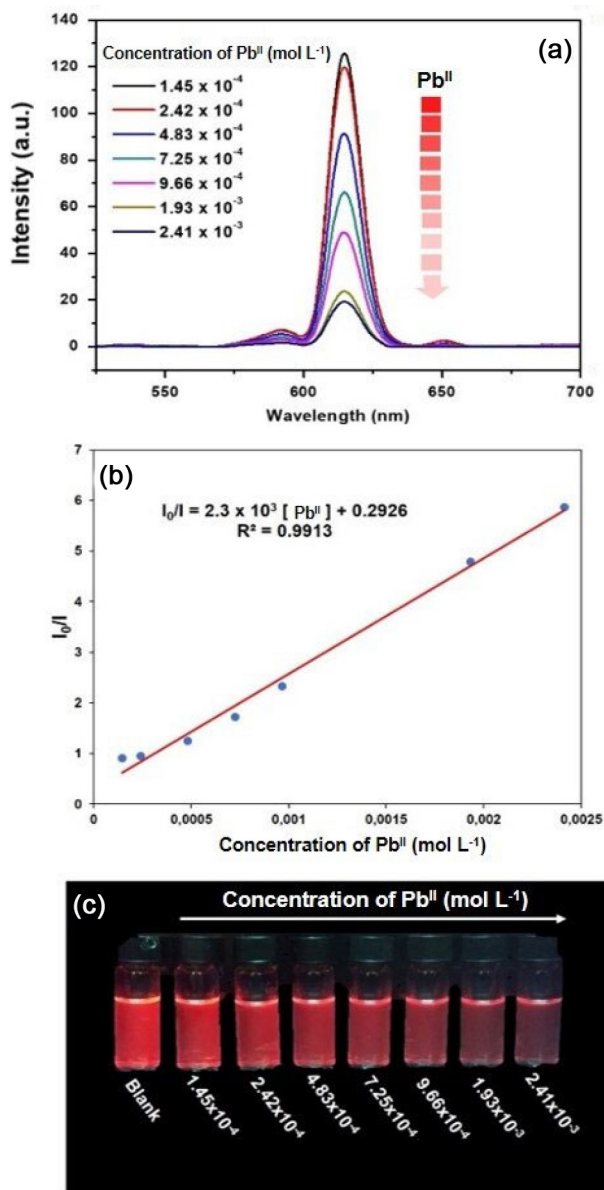


Figure 4. (a) Emission spectra ($\lambda_{\text{ex}} = 375$ nm) monitoring the intensity of the ${}^5\text{D}_0 \rightarrow {}^7\text{F}_2$ transition (at 612 nm) of $[\text{Eu}(\text{TTA})_3(2\text{-pyr})(\text{H}_2\text{O})]$ in aqueous solution with Pb^{II} at different concentrations (b) *versus* I_0/I , and (c) luminescence of the mixtures with Pb^{II} at different concentrations, illuminated with a UV lamp at 365 nm at room temperature.

the increase in Pb^{II} concentration (Figure 4). The greater quenching caused by Pb^{II} may be explained by the energy absorption competition at the same wavelength of the ligand or by the complex- Pb^{II} interaction. The UV-Vis absorption spectrum of Pb^{II} in aqueous solution (Figure S5, SI section) showed an overlap with the complex excitation spectrum (Figure 2a), evincing the absorption competition between Pb^{II} and the europium(III) complex. Moreover, Pb^{II} ion electronic state has an empty p orbital, making it prone to become an electron-acceptor and thus weakening fluorescence.^{75,76}

The ratio I_0/I *versus* Pb^{II} concentration (Figure 4b) provides a coefficient of determination, $R^2 = 0.9913$, and the

equation may be adjusted as $(I_0/I) - 1 = 2.3 \times 10^3 [\text{Pb}^{\text{II}}] - 0.7074$. With that, the ratio approaches the Stern-Volmer equation: $(I_0/I) - 1 = K_{\text{SV}}[\text{M}]$, where I_0 and I are the ${}^5\text{D}_0 \rightarrow {}^7\text{F}_2$ band emission intensities before and after metal addition, respectively; $[\text{M}]$ is the molar concentration of the metal ion; and K_{SV} is a Stern-Volmer constant that indicates quenching intensity.⁷⁷ Based on the approximation, the K_{SV} value for $[\text{Eu}(\text{TTA})_3(2\text{-pyr})(\text{H}_2\text{O})]$ in the presence of Pb^{II} was equal to 2300 L mol^{-1} . Limit of detection (LOD) was calculated using the equation $\text{LOD} = 3\sigma/k$, where σ is the blank measurement standard deviation and k is the slope (I_0/I) vs. $[\text{Pb}^{\text{II}}]$,⁷⁸ reaching the value of 6.03 μM . In a study conducted by Lin *et al.*,⁷⁹ the authors evaluated an europium(III) coordination polymer as a sensor for Pb^{II} , finding K_{SV} to be equal to 33014 L mol^{-1} and LOD to 90.78 μM in water. Lin *et al.*⁷⁹ synthesized europium(III) coordination polymer Eu-CPs, $\{[\text{Eu}_2(\text{PBA})_3(\text{H}_2\text{O})_3] \cdot \text{DMF} \cdot 3\text{H}_2\text{O}\}_n$, this compound exhibited 3D framework, what increases the weak bonding interaction between nitrogen atoms and Pb^{II} . This interaction perturbs the electronic structure of the ligand and reduce the energy transfer efficiency from the ligand to Eu^{III} centers. In the present work $[\text{Eu}(\text{TTA})_3(2\text{-pyr})(\text{H}_2\text{O})]$ compound did not exhibit 3D framework.

Sensor to detect ethanol in gasoline

To evaluate the effect of the gasoline (ethanol mixture in the 0-100% (v/v) range) on the luminescence of the complex, we monitored the ${}^5\text{D}_0 \rightarrow {}^7\text{F}_2$ transition (612 nm) in the emission spectra (Figure 5a) of $[\text{Eu}(\text{TTA})_3(2\text{-pyr})(\text{H}_2\text{O})]$ in the ethanol-gasoline mixture (% v/v). The increase in the proportion of gasoline by ethanol volume significantly affected the ${}^5\text{D}_0 \rightarrow {}^7\text{F}_2$ transition, increasing luminescence (Figure 5a). This may be explained by the fact that the chemical environment where the complex is located consists mostly of an apolar solvent, minimizing energy losses by a non-radioactive process. Quenching probability through OH oscillators resonance increases with a greater amount of ethanol,⁵ as shown in Figure 5b.

The ethanol-gasoline mixtures (% v/v) (Figure 5b) presented the characteristic luminescence of the complex in the red region when illuminated with a UV lamp (at 365 nm). Based on the regulation that determines the permitted volume of ethanol in gasoline,⁸⁰ we blended ethanol in the following concentrations: 20, 30, 40, 50, and 60% v/v. Concentrations were related by the I_0/I ratio, where I_0 and I are the emission intensities of the ${}^5\text{D}_0 \rightarrow {}^7\text{F}_2$ band before and after adding ethanol to gasoline, respectively. With that, we obtained a determination coefficient (R^2) equal to 0.9815, and calculated LOD (4.94% v/v) using the following equation: $\text{LOD} = 3\sigma/k$, where σ is the

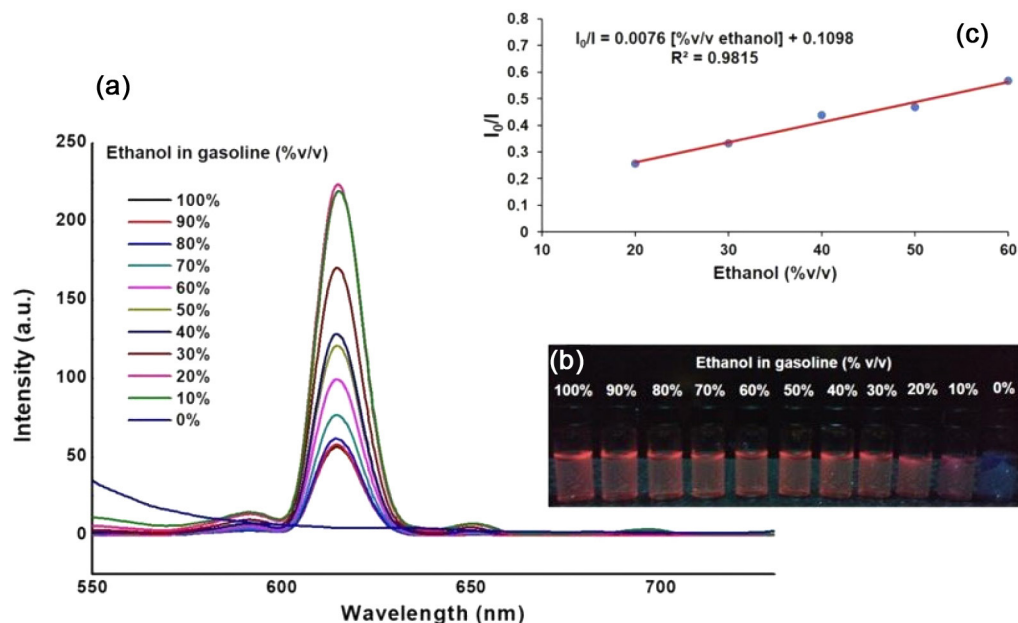


Figure 5. (a) Emission spectra ($\lambda_{ex} = 375$ nm) monitoring the intensity of the ${}^5D_0 \rightarrow {}^7F_2$ transition (612 nm) of $[\text{Eu}(\text{TTA})_3(2\text{-pyr})(\text{H}_2\text{O})]$ in the ethanol-gasoline mixture (% v/v). (b) Luminescence of the complex mixed with different volumes of ethanol in gasoline, under ultraviolet irradiation at 365 nm at room temperature and (c) I_0/I ratio versus ethanol concentration in gasoline (% v/v).

blank measurement standard deviation and k is the slope (I_0/I) vs. ethanol (% v/v).⁷⁸ Our results indicate that using the complex as a luminescent marker to identify ethanol in gasoline is a promising alternative for fuel quality control.

Conclusions

Our study verified that the use of $[\text{Eu}(\text{TTA})_3(2\text{-pyr})(\text{H}_2\text{O})]$ complex as luminescent sensor is a promising alternative for detecting Pb^{II} . We evaluated Pb^{II} concentration based on the luminescence quenching of the complex, finding a great sensitivity based on the values found for $K_{SV} = 2300 \text{ L mol}^{-1}$, $R^2 = 0.9913$, and $\text{LOD} = 6.03 \mu\text{M}$. Our results reveal that the complex could be used for identifying and quantifying Pb^{II} . We also tested the use of the complex as a luminescent marker to identify gasoline adulteration with the addition of ethanol, reaching the values of $R^2 = 0.9815$ and $\text{LOD} = 4.94\%$ v/v. These values indicate that the complex is sensitive and efficient, being promising for fuel quality control.

Supplementary Information

Supplementary data (spectral data, FTIR and UV-Vis, TG/DTG, and DTA) are available free of charge at <http://jbcbs.s bq.org.br> as a PDF file.

Acknowledgments

The authors thank CAPES (23038.007083/2014-40), FAPES (edital CNPq/FAPES No. 23/2018, Programa de

Apoio a Núcleos Emergentes, PRONEM), and CNPq (422555/2018-5, and 305359/2017-7) for financial support. The authors would also like to thank the Núcleo de Competências em Química do Petróleo and LabPetro for the use of their installations. This study was financed in part by the Coordenação de Aperfeiçoamento de Pessoal de Nível Superior, Brasil (CAPES) - Finance Code 1.

Author Contributions

Clebson de J. Macrino was responsible for the conceptualization, data curation, formal analysis, investigation, methodology, visualization, writing the original draft, review, and editing; Alex dos S. Borges for the conceptualization, data curation, formal analysis, investigation, methodology, visualization, writing the original draft, and review; Álvaro C. Neto for the conceptualization, data curation, formal analysis, investigation, methodology, visualization, writing the original draft, and review; Valdemar Lacerda Jr. and Wanderson Romão were responsible for the conceptualization, funding acquisition, investigation, methodology, project administration, resources, supervision; visualization, writing the original draft, review, and editing.

References

1. Rostra, J. G.; Ferrer, F. J.; Espinós, J. P.; Elipe, A. R. G.; Yubero, E.; *ACS Appl. Mater. Interfaces* **2017**, *9*, 16313.
2. Du, P.; Bharat, L. K.; Yu, J. S.; *J. Alloys Compd.* **2015**, *633*, 37.
3. Ling, Q.; Song, Y.; Ding, S. J.; Zhu, C.; Chan, D. S. H.; Kwong, D. L.; Kang, E. T.; Neoh, K. G.; *Adv. Mater.* **2005**, *17*, 455.

4. Reichardt, C.; Schneider, K. R. A.; Sainuddin, T.; Wächtler, M.; McFarland, S. A.; Dietzek, B.; *J. Phys. Chem. A* **2017**, *121*, 5635.
5. Muller, G.; *Dalton Trans.* **2009**, *44*, 9692.
6. Jia, J.; Zhang, Y.; Zheng, M.; Shan, C.; Yan, H.; Wu, W.; Gao, X.; Cheng, B.; Liu, W.; Tang, Y.; *Inorg. Chem.* **2018**, *57*, 300.
7. Kumar, P.; Kanika; Singh, S.; Lahon, R.; Gundimeda, A.; Gupta, G.; Gupta, B. K.; *J. Lumin.* **2018**, *196*, 207.
8. Kunczewicz, J.; Dąbrowski, J. M.; Kyzioł, A.; Brindell, M.; Łabuz, P.; Mazuryk, O.; Macyk, W.; Stochel, G.; *Coord. Chem. Rev.* **2019**, *398*, 113012.
9. Kariaka, N. S.; Smola, S. S.; Rusakova, N. V.; Dyakonenko, V. V.; Shishkina, S. V.; Sliva, T. Y.; Trush, V. A.; Amirhanov, V. M.; *J. Lumin.* **2020**, *223*, 117187.
10. Rosa, P. P. F.; Kitagawa, Y.; Hasegawa, Y.; *Coord. Chem. Rev.* **2020**, *406*, 213153.
11. Cotton, S. A.; Raithby, P. R.; *Coord. Chem. Rev.* **2017**, *340*, 220.
12. You, L. X.; Hao, J. H.; Qi, D.; Xie, S. Y.; Wang, S. J.; Xiong, G.; Dragutan, I.; Dragutan, V.; Ding, F.; Sun, Y. G.; *Inorg. Chim. Acta* **2019**, *497*, 119075.
13. Karraker, D. G.; *J. Chem. Educ.* **1970**, *47*, 424.
14. Yanagisawa, K.; Nakanishi, T.; Kitagawa, Y.; Seki, T.; Akama, T.; Kobayashi, M.; Taketsugu, T.; Ito, H.; Fushimi, K.; Hasegawa, Y.; *Eur. J. Inorg. Chem.* **2015**, *28*, 4769.
15. Burdett, J. K.; Hoffmann, R.; Fay, R. C.; *Inorg. Chem.* **1978**, *17*, 2553.
16. Kuramochi, Y.; Nakagawa, T.; Yokoo, T.; Yuasa, J.; Kawai, T.; Hasegawa, Y.; *Dalton Trans.* **2012**, *41*, 6634.
17. Bünzli, J. C. G.; Chauvin, A. S.; Vandevyver, C. D. B.; Bo, S.; Comby, S.; *Ann. N. Y. Acad. Sci.* **2008**, *1130*, 97.
18. Heffern, M. C.; Matosziuk, L. M.; Meade, T. J.; *Chem. Rev.* **2014**, *114*, 4496.
19. Braun, F.; Comba, P.; Grimm, L.; Herten, D. P.; Pokrandt, B.; Wadepohl, H.; *Inorg. Chim. Acta* **2018**, *484*, 464.
20. Zhang, J. W.; Wang, C. R.; Liu, W. H.; Xu, S.; Liu, B. Q.; *Inorg. Chim. Acta* **2020**, *508*, 119648.
21. Bai, C.; Fu, X. Y.; Hu, H. M.; He, S.; Wang, X.; Xue, G. L.; *Inorg. Chim. Acta* **2020**, *506*, 119550.
22. Chen, W. T.; *J. Solid State Chem.* **2019**, *284*, 121160.
23. Ning, Y.; Zhu, M.; Zhang, J. L.; *Coord. Chem. Rev.* **2019**, *399*, 213028.
24. Abdelhamid, H. N.; Wilk-Kozubek, M.; El-Zohry, A. M.; Gómez, A. B.; Valiente, A.; Martín-Matute, B.; Mudring, A. V.; Zou, X.; *Microporous Mesoporous Mater.* **2019**, *279*, 400.
25. Jia, J. H.; Li, Q. W.; Chen, Y. C.; Liu, J. L.; Tong, M. L.; *Coord. Chem. Rev.* **2019**, *378*, 365.
26. Maouche, R.; Belaid, S.; Benmerad, B.; Bouacida, S.; Freslon, S.; Daiguebonne, C.; Suffren, Y.; Calvez, G.; Bernot, K.; Roiland, C.; Pollès, L.; Guillou, O.; *Inorg. Chim. Acta* **2020**, *501*, 119309.
27. Sun, Y.; Li, Q.; Wei, S.; Zhao, R.; Han, J.; Ping, G.; *J. Lumin.* **2020**, *225*, 117241.
28. Stan, C. S.; Rosca, I.; Sutiman, D.; Secula, M. S.; *J. Rare Earths* **2012**, *30*, 401.
29. Zhao, Y.; Wang, S.; Han, Y.; Zhang, J.; Liu, C.; Hu, X.; Zhang, Z.; Wang, L.; *J. Lumin.* **2020**, *223*, 117253.
30. Yang, D.; Liao, L.; Zhang, Y.; Guo, Q.; Mei, L.; Liu, H.; *J. Lumin.* **2020**, *224*, 117285.
31. Baklanova, Y. V.; Maksimova, L. G.; Lipina, O. A.; Tyutyunnik, A. P.; Zubkov, V. G.; *J. Lumin.* **2020**, *224*, 117315.
32. Herrmann, A.; Friedrich, D.; Zschechel, T.; Rüssel, C.; *J. Lumin.* **2019**, *214*, 116550.
33. Kaczmarek, M.; *J. Lumin.* **2020**, *222*, 117174.
34. Binnemans, K.; *Chem. Rev.* **2009**, *109*, 4283.
35. Sizov, V. S.; Komissar, D. A.; Metlina, D. A.; Aminev, D. F.; Ambrozevich, S. A.; Nefedov, S. E.; Varaksina, E. A.; Metlin, M. T.; Mislavskii, V. V.; Taydakova, I. V.; *Spectrochim. Acta, Part A* **2020**, *225*, 117503.
36. Duan, Y. Y.; Wu, D. F.; Chen, H. H.; Wang, Y. J.; Li, L.; Gao, H. L.; Cu, J. Z.; *Inorg. Chim. Acta* **2020**, *499*, 119203.
37. Bereznytska, O. S.; Savchenko, I. O.; Ivakha, N. B.; Rogovtsov, O. O.; Trunova, O. K.; Rusakova, N. V.; *J. Mol. Struct.* **2020**, *1201*, 127160.
38. Bhat, S. A.; Iftikhar, K.; *Dyes Pigm.* **2020**, *179*, 108383.
39. Borges, A. S.; Fulgêncio, F.; Silva, J. G.; Santos, T. A. R.; Diniz, R.; Windmöller, D.; Magalhães, W. F.; Araujo, M. H.; *J. Lumin.* **2019**, *205*, 72.
40. Borges, A. S.; Caliman, E. V.; Dutra, J. D. L.; Silva, J. G.; Araujo, M. H.; *J. Lumin.* **2016**, *170*, 654.
41. Lucena, M. A. M.; Sá, G. F.; Rodrigues, M. O.; Alves, S.; Talhavini, M.; Weber, I. T.; *Anal. Methods* **2013**, *5*, 705.
42. Destefani, C. A.; Motta, L. C.; Costa, R. A.; Macrino, C. J.; Bassane, J. F. P.; Filho, J. F. A.; Silva, E. M.; Greco, S. J.; Carneiro, M. T. W. D.; Endringer, D. C.; Romão, W.; *Microchem. J.* **2016**, *124*, 195.
43. Devi, R.; Rajendran, M.; Singh, K.; Pala, R.; Vaidyanathan, S.; *J. Mater. Chem. C* **2021**, *9*, 6618.
44. Wang, Q.; Long, M. Y.; Lv, C. Y.; Xin, S. P.; Han, X. G.; Jiang, W.; *Food Control* **2020**, *109*, 106894.
45. Zmojda, J.; Kochanowicz, M.; Miluski, P.; Golonko, P.; Baranowska, A.; Ragi, T.; Dorosz, J.; Kuwik, M.; Pisarski, W.; Pisarska, J.; Szal, R.; Mach, G.; Starzyk, B.; Lesniak, M.; Sitarz, M.; Dorosz, D.; *Materials* **2020**, *13*, 2817.
46. Zhang, D.; Zhang, Y.; Wang, Z.; Zheng, Y.; Zheng, X.; Gao, L.; Wang, C.; Yang, C.; Tang, H.; Li, Y.; *J. Lumin.* **2021**, *229*, 117706.
47. Li, R. F.; Zhang, T.; Liu, X. F.; Feng, X.; *Inorg. Chem. Commun.* **2016**, *73*, 170.
48. Zhou, J.; Li, B.; Qi, A.; Shi, Y.; Qi, J.; Xu, H.; Chen, L.; *Sens. Actuators, B* **2019**, *305*, 127462.

49. Sun, Z.; Li, H.; Sun, G.; Guo, J.; Ma, Y.; Li, L.; *Inorg. Chim. Acta* **2018**, *469*, 51.
50. Chen, Z.; Yu, X.; Li, X.; Ye, Q.; Zhou, K.; Cai, Y.; Huang, L.; Li, Y.; Zeng, C.; *Inorg. Chem. Commun.* **2020**, *112*, 107744.
51. Zhang, F.; Ma, J.; Huang, S.; Li, Y.; *Spectrochim. Acta, Part A* **2020**, *228*, 117816.
52. Zhai, B.; Li, Z. Y.; Wub, Z. L.; Cui, J. Z.; *Inorg. Chem. Commun.* **2016**, *71*, 23.
53. Li, R.; Zhang, Y.; Liu, X.; Chang, X.; Feng, X.; *Inorg. Chim. Acta* **2020**, *502*, 119370.
54. Zheng, M.; Tan, H.; Xie, Z.; Zhang, L.; Jing, X.; Sun, Z.; *ACS Appl. Mater. Interfaces* **2013**, *5*, 1078.
55. Yan, Q.; Chen, Z. H.; Xue, S. F.; Han, X. Y.; Lin, Z. Y.; Zhang, S.; Shi, G.; Zhang, M.; *Sens. Actuators, B* **2020**, *268*, 108.
56. Xu, X. Y.; Yan, B.; *Sens. Actuators, B* **2016**, *222*, 347.
57. Lou, T.; Chen, Z.; Wang, Y.; Chen, L.; *ACS Appl. Mater. Interfaces* **2011**, *3*, 1568.
58. Lian, C.; Chen, Y.; Li, S.; Hao, M.; Gao, F.; Yang, L.; *J. Alloys Compd.* **2017**, *702*, 303.
59. Yang, L.; Song, S.; Zhang, H.; Zhang, W.; Bu, Z.; Ren, T.; *Synth. Met.* **2011**, *161*, 2230.
60. Fonseca, R. R. F.; Gaspar, R. D. L.; Raimundo Jr., I. M.; Luz, P. P.; *J. Rare Earths* **2019**, *37*, 225.
61. Xue, B.; Zhang, Z.; Sund, Y.; Wang, J.; Jiang, H.; Du, M.; Chi, C.; Li, X.; *Carbohydr. Polym.* **2018**, *186*, 176.
62. Teotonio, E. E. S.; Fett, G. M.; Brito, H. F.; Sá, W. M. F. G. F.; Felinto, M. C. F. C.; Santos, R. H. A.; *J. Lumin.* **2008**, *128*, 190.
63. Li, Y. J.; Yan, B.; Li, Y.; *Microporous Mesoporous Mater.* **2010**, *131*, 82.
64. Li, Y.; Jiao, J.; Yan, P.; Liu, L.; Wang, J.; Wang, Y.; Huang, L.; Liu, J.; Belfiore, L. A.; *Scr. Mater.* **2018**, *152*, 1.
65. Charles, R. G.; Ohlmann, R. C.; *J. Inorg. Nucl. Chem.* **1965**, *27*, 255.
66. Zou, Y.; Wang, X.; Khan, A.; Wang, P.; Liu, Y.; Alsaedi, A.; Hayat, T.; Wang, X.; *Environ. Sci. Technol.* **2016**, *50*, 7290.
67. Wu, D.; Chen, L.; Lee, W.; Ko, G.; Yin, J.; Yoon, J.; *Coord. Chem. Rev.* **2018**, *354*, 74.
68. Lyle, S. J.; Rahaman, M. M.; *Talanta* **1963**, *10*, 1177.
69. Ugale, A.; Kalyani, N. T.; Dhoble, S. J.; *Mater. Sci. Energy Technol.* **2020**, *3*, 51.
70. Oliveira, T. C.; Santos, H. P.; Lahoud, M. G.; Franco, D. F.; Freire, R. O.; Dutra, J. D. L.; Cuin, A.; Lima, J. F.; Marques, F. L.; *J. Lumin.* **2017**, *181*, 196.
71. Chitnis, D.; Kalyani, N. T.; Dhoble, S. J.; *Optik* **2017**, *130*, 237.
72. Marques, L. F.; Santos, H. P.; Oliveira, K. A.; Botezine, N. P.; Freitas, M. C. R.; Freire, R. O.; Dutra, J. D. L.; Martins, J. S.; Legnani, C.; Quirino, W. G.; Machado, F. C.; *Inorg. Chim. Acta* **2016**, *458*, 28.
73. Donegá, C. D.; Alves Jr., S.; Sá, G. F.; *J. Alloys Compd.* **1997**, *250*, 422.
74. Marques, L. F.; Cuin, A.; Carvalho, G. S. G.; Santos, M. V.; Ribeiro, S. J. L.; Machado, F. C.; *Inorg. Chim. Acta* **2016**, *441*, 67.
75. Yan, Y. T.; Zhang, W. Y.; Zhang, F.; Cao, F.; Yang, R. F.; Wang, Y. Y.; Hou, L.; *Dalton Trans.* **2018**, *47*, 1682.
76. Song, X. Z.; Wang, Y. X.; Yan, J. W.; Chen, X.; Meng, Y. L.; Tan, Z.; *ChemistrySelect* **2018**, *3*, 9564.
77. Zeng, X.; Zhang, Y.; Zhang, J.; Hu, H.; Wu, X.; Long, Z.; Hou, X.; *Microchem. J.* **2017**, *134*, 140.
78. Zhang, M. H.; Zhang, L. L.; Xiao, Z. Y.; Zhang, Q. H.; Wang, R. M.; Dai, F. N.; Sun, D. F.; *Sci. Rep.* **2016**, *6*, 20672.
79. Lin, J.; Cheng, Q.; Zhou, J.; Lin, X.; Reddy, R. C. K.; Yang, T.; Zhang, G.; *J. Solid State Chem.* **2019**, *270*, 339.
80. Romanel, S. A.; Cunha, D. A.; Castro, E. V. R.; Barbosa, L. L.; *Microchem. J.* **2018**, *140*, 31.

Submitted: June 9, 2021

Published online: September 27, 2021

